Effect of Infiltration of Barium Carbonate Nanoparticles on Electrochemical Performance of $La_{0.6}Sr_{0.4}Co_{0.2}Fe_{0.8}O_{3-\delta}$ Cathode for Protonic Ceramic Fuel Cells

Jun Gao, Yuqing Meng, Jianhua Tong, Kyle S. Brinkman[a,b]
[a]Department of Materials Science and Engineering, Clemson University, Clemson, SC 29634, USA

Shiwoo Lee[b,c]
[b]U. S. Department of Energy, National Energy Technology Laboratory, Morgantown, WV 26507, USA
[c]AECOM, Morgantown, WV 26507, USA

Keywords: Oxygen reduction reaction, Proton ceramic fuel cell, infiltration

Abstract

$BaCO_3$ nanoparticles were infiltrated on a $La_{0.6}Sr_{0.4}Co_{0.2}Fe_{0.8}O_{3-\delta}$ (LSCF) electrode as a synergistic catalyst for enhancing the performance of proton conducting solid oxide fuel cells (H-SOFCs). Electrochemical impedance analysis showed that the polarization resistance dramatically reduced from 1.123 to 0.293 Ω•cm^2 at 700 ºC (nearly 75% decrease of the polarization resistance) after infiltration of the $BaCO_3$ nanoparticles. The chemical stability between the $BaCO_3$ and LSCF electrode was investigated by running a 300 h long-term test where the polarization resistance exhibited a minor degradation (2.22 to 2.20 Ω•cm^2). In addition, single cells with infiltrated LSCF electrode and a $BaCe_{0.7}Zr_{0.1}Y_{0.1}Yb_{0.1}O_{3-\delta}$ (BCZYYb) electrolyte yielded a maximum power density of 404 mW•cm^{-2} at 700 ºC, which is much higher than cells with bare LSCF electrode (268 mW•cm^{-2} at 700 ºC). $BaCO_3$ demonstrated promising performance enhancements of LSCF electrodes in H-SOFCs and warrants further development.

Introduction

Solid oxide fuel cells (SOFCs) efficiently convert the chemical energy in fuels into electricity with limited by-products[1] [2] [3] [4]. However, the elevated working temperature (800-1000℃), and the long term performance/durability are the main obstacles limiting practical applications. Proton-conducting SOFCs (H-SOFCs) has attracted more interest in recent years due to the lower working temperatures (400-700℃) and a lower activation energy for proton transport as compared to oxygen ion systems[5].

For a given electrolyte with a specific thickness, the chemical reaction process in the cathode is the main factor that determine the performance of the SOFC. To improve the oxygen reduction reaction(ORR) in the cathode, two approaches have been utilized: i) compositional modifications such as Haile and Shao [6] who pioneered the high performance $Ba_{0.5}Sr_{0.5}Co_{0.8}Fe_{0.2}O_{3-\delta}$ (BSCF) cathode and

ii) optimization of the electrode microstructure. For example, synthesis methods such as the phase inversion method have been employed to produce aligned pores to reduce the diffusion barrier [7]. Another additional method which combines compositional and microstructural modifications is the infiltration method to achieve a nano-scale electrode with an enlarged the area for catalytic reaction [8] [9].

Significant work has been performed on the oxygen ion SOFCs (O-SOFCs) by infiltration of nanoparticles to increase its oxygen catalytic active in the cathode. However, limited work to-date has focused on improving the cathode performance of H-SOFCs through infiltration. $La_{0.6}Sr_{0.4}Co_{0.2}Fe_{0.8}O_{3-\delta}$ (LSCF) is a widely used cathode with excellent mixed electronic and ionic conductivity at intermediate temperatures [10] [11], but suffer low electronic conductivity at low temperatures. Libin Lei [12] reported $PrNi_{0.5}Mn_{0.5}O_3$ and PrOx as infiltration materials in the LSCF electrode of H-SOFCs indicating that the hybrid catalyst significantly improves the cathode reaction kinetics and fuel cell performance. Geng Li [13] infiltrated the oxygen ion conductor $Y_{0.25}Bi_{0.75}O_{1.5}$ in a LSCF electrode resulting in decreased interfacial polarization resistance. Beibei He *et.al* [14] deposited $Gd_{0.1}Ce_{0.9}O_{1.95}$ nano-particles in a LSCF electrode resulting in a polarization resistance decreased from 10.77 to 2.47 Ω cm^2 at 600 ºC.

Infiltration of alternative materials such as alkali earth metals compounds $BaCO_3$[15], $SrCO_3$ [16], CaO [17], MgO [18], is another strategy used to improve the performance of the cathode which has been proved effective in O-SOFCs. For example, the polarization resistance decreased from 0.4 to 0.16 Ω cm^2 at 700 ºC for LSCF electrode with $BaCO_3$ infiltration. When $SrCO_3$ nanoparticles was used as the synergetic catalyst, the cell performance increased by a factor of 1.9.

In this work, we report the catalytic activity of $BaCO_3$ nanoparticles on LSCF cathode, which are formed by thermal decomposition of barium acetate, $Ba(Ac)_2$. Electrochemical impedance spectroscopy (EIS) was applied to investigate the reduction of interfacial polarization resistance of LSCF electrode on a $BaCe_{0.7}Zr_{0.1}Y_{0.1}Yb_{0.1}O_{3-\delta}$ (BCZYYb) electrolyte, and the extended long-term test showed the chemical stability of $BaCO_3$ nanoparticles on LSCF cathode. Furthermore, an excellent single cell performance was achieved with optimized $BaCO_3$ loading.

Experimental

Powder preparation

LSCF powder was synthesized using an EDTA-citric combustion method [19]. Stoichiometric amounts of the precursors $La(NO_3)_3$, $Sr(NO_3)_2$, $Co(NO_3)_3$ and $Fe(NO_3)_3$ (99.5% Sinopharm Chemical Reagent Co.) were dissolved in distilled water and then citric and EDTA added in the solution with a ratio of 1:1:1, metal/citric acid/EDTA as the chelating agent to assist the combustion process. The precursor solution followed by heated on a hot plate until self-combustion occurred. The acquired powder was then calcinated at 800 ºC for 2 h to remove the organic residue in the ashes and to form a perovskite structure.

The BCZYYb electrolyte precursor powder and 40 wt.% BCZYYb + 60 wt.% NiO anode precursor powder was prepared by simple mixing and drying process. For electrolyte precursor powder, stoichiometric amount of $BaCO_3$, CeO_2, ZrO_2, Y_2O_3, Yb_2O_3 with the addition of 1.0 wt.% NiO as a sintering aid were mixed together in isopropanol with 3mm YSZ (yttria-stabilized zirconia) beads for 48 h, followed by drying at 90 ºC for 24 h. For anode precursor powder, proper amounts of $BaCO_3$, CeO_2, ZrO_2,Y_2O_3, Yb_2O_3 with 20 wt.% starch as the pore-former were blended unsing the same ball-milling and dryimg procedures used for the electrolyte precursor.

Cell Fabrication

For the LSCF symmetrical cells, the electrolyte dense pellets were synthesized by a cost-effective solid-state sintering method [20].The electrolyte precursor powder was dry-pressed under 250 MPa for 1 minute in a circular carbon-aided steel die with a diameter of 15 mm to get green electrolyte pellets. The green pellet was sintered at 1450 ºC for 12 h to obtain a dense electrolyte, followed by polishing. The LSCF slurries were prepared by mixing the LSCF powders with an organic binder and dispersant. The as-prepared slurry was printed on both sides of the BCZYYb pellets. After dried by infrared lamp, the symmetrical cell was obtained by heating at 1050 ºC for 2 h.

For the single cells, the anode precursor powder was dry-pressed under 160 MPa for a minute in a circular carbon-aided steel die with a diameter of 19 mm to produce green anode pellets. The electrolyte precursor powder was mixed with binder and dispersant to form the electrolyte slurry and subsequently deposited on each side of the green anode pellets by screen-printing followed by co-sintering at 1450 ºC for 12 h. The as prepared LSCF slurry was printed on the electrolyte side and sintered at 1050 ºC for 2 h to obtain the full cell.

Stoichiometric amounts of barium acetate, $Ba(Ac)_2$ (Alfa Aesar 99%, Co. Ltd) were dissolved in water to form a 0.3 mol L^{-1} solution. Different amounts of $Ba(Ac)_2$ were infiltrated in the LSCF electrode and fired at 800 ºC in air for 1 h to form the $BaCO_3$ nanoparticle catalyst.

Microstructure of cathodes

The microstructure of the $BaCO_3$ infiltrated cathode and the morphology of single cell were revealed by using scanning electron -spectroscopy (SEM).

Electrochemical Measurements

The electrochemical performance of cathode was tested using symmetrical fuel cells from 550 ºC to 700 ºC. Silver paste was printed onto both surface of electrode, working as the current collectors. Electrochemical impedance spectra were obtained by electrochemical workstation (Solartron®, SI 1287 + 1260) with an AC amplitude of 10 mV in the frequency range from 1MHz to 10 mHz. AC impedance plots were fitted by using Zview software according to the equivalent circuit. The performance of single cells was tested with cathode exposed to dry air and anode to humified (3% H_2O) hydrogen. Single cells were sealed in an aluminum tube by ceramic bond, and the silver wires were used as the voltage and current leads.

Results and discussion

Formation of $BaCO_3$ nanoparticles on the LSCF surface

Figure 1a shows the SEM micrographs of the LSCF electrode on a dense BCZYYb electrolyte. The representative porous electrode exhibited a good interfacial connection with the electrolyte and revealed a fine microstructure with nearly 0.2 μm grain size. No apparent pores were observed in the dense electrolyte. Figure 1b and 1c show the distribution of the $BaCO_3$ nanoparticles on the LSCF electrode. Nanoscale $BaCO_3$ particles were uniformly deposited on the LSCF grain surface with a particle size of approximately 20-30 nm. No aggregation or coarsening of the nanoparticles was observed to occur during fabrication of the cell.

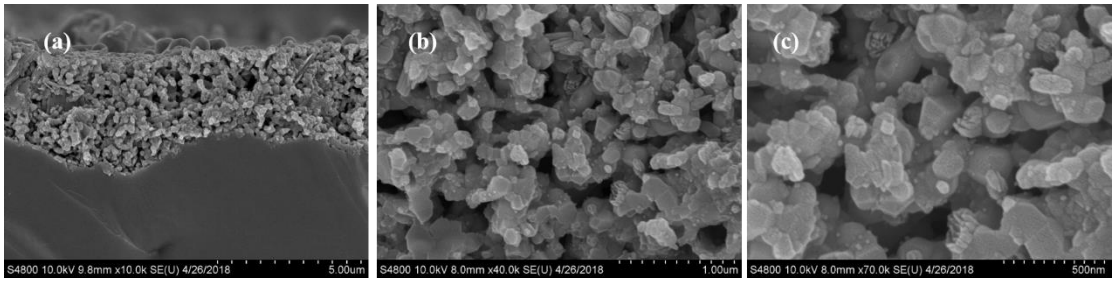

Figure 1. Microstructure of a) LSCF electrode and BCZYYb electrolyte and b,c) 8.74 wt.% $BaCO_3$ nanoparticles on the LSCF electrode

Representative EIS of different loadings of $BaCO_3$ at different temperatures

The catalytic effect was demonstrated on the composite electrodes infiltrated with different amounts of $BaCO_3$ particles. Symmetrical cells with varying amounts of $BaCO_3$ loading demonstrated reduced polarization resistance over the entire testing temperature, from 700 to 600 ºC as compared to the bare LSCF electrode. Note that both high and low loadings of $BaCO_3$ resulted in a decrease of the polarization resistance. The lowest polarization resistance was achieved with 8.74 wt.% $BaCO_3$ at different temperatures. For example, the polarization resistance decreased by nearly 75% (1.123 to 0.293 Ω•cm^2 at 700 ºC) which demonstrated catalytic activity for the ORR in LSCF electrodes. Elevating coverage and connectivity of the infiltrated nanoparticles causes the gradual reduction in polarization resistance for the electrodes with single-digit weight percentage $BaCO_3$. The decrease of the arc at the mid-frequency range (or the second arc from the high frequency intercept on the real axis) indicates surface reaction process in the electrodes is improved by the infiltration. Further addition of $BaCO_3$ may affect diffusion of gases to active sites. The tails of the impedance spectra at the low frequency range, shown for the cathode with 12.02 wt% $BaCO_3$, may indicate the presence of concentration polarization by excess loading.

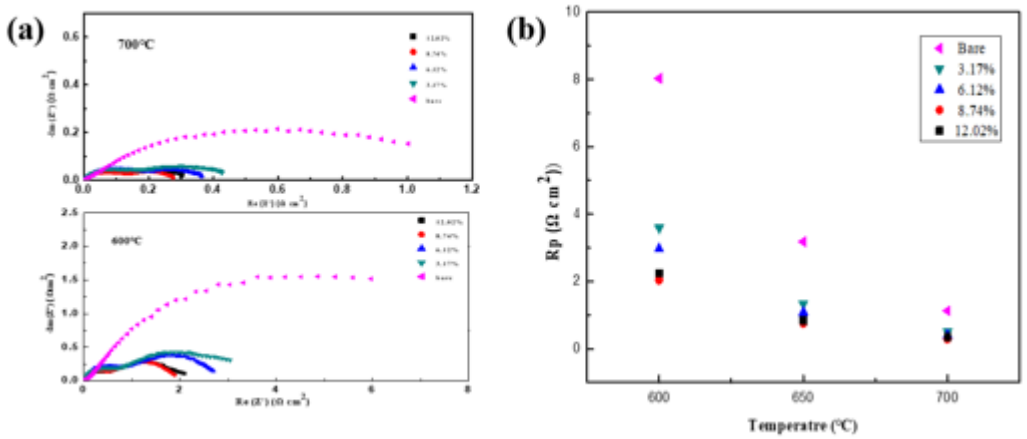

Figure 2. Representative EIS results of LSCF symmetrical cells with different BaCO3 loadings at (a) 700°C and (b) 600°C; (c) Comparison of polarization resistance of symmetrical cells with different BaCO3 loadings from 700°C to 600°C.

The long-term stability of optimize symmetrical cell

Figure 3 shows the long-term stability of the optimized symmetrical fuel cells at 600 ºC indicating negligible degradation over the durations examined in this work. The interfacial polarization resistance remained stable over the nearly 300 h testing, from 2.22 Ω•cm^2 to 2.20 Ω•cm^2. This indicates the material $BaCO_3$ is stable on the LSCF backbone with limited reaction between the $BaCO_3$ particles and LSCF electrode, and limited agglomeration or coarsening of the $BaCO_3$ nanoparticles.

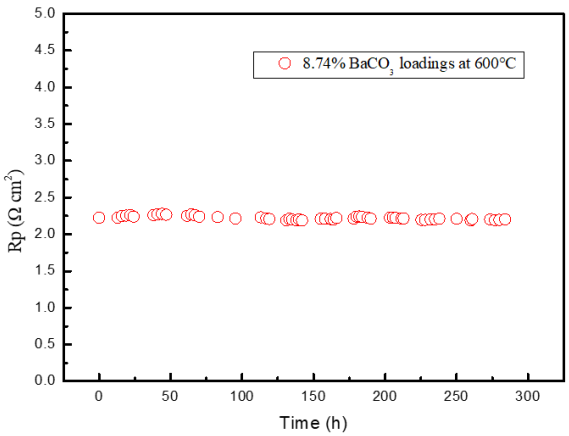

Figure 3. Polarization resistance of the LSCF electrode with 8.74 wt.% $BaCO_3$ after extended testing at 600 ºC for nearly 300 h

This result could be further estimated by the microstructure of the $BaCO_3$ nanoparticles before and after the long-term test displayed in Figure 4. The size of the nanoscale $BaCO_3$ was approximately 40 nm, a slight increase as compared to the as-fabricated samples. It indicates the $BaCO_3$ nanoparticle maintained the shape and crystalline structure after 300 h at 600 ºC providing a potential solution for long term proton conducting fuel cells applications.

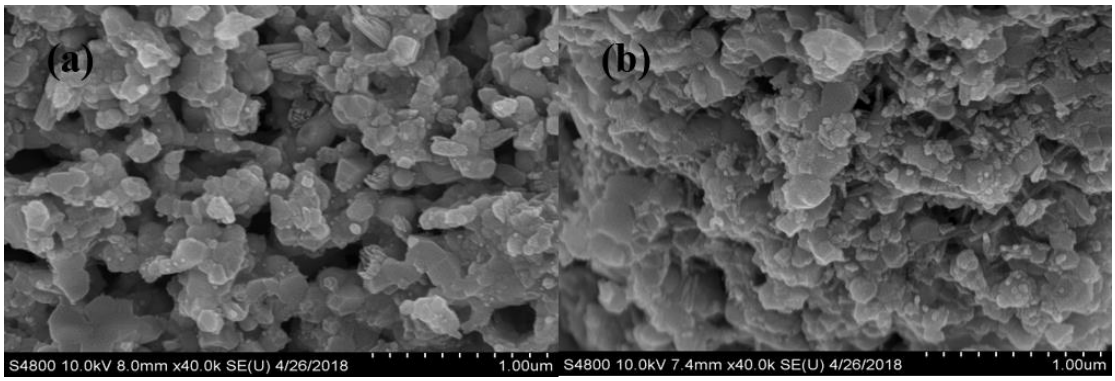

Figure 4. The microstructure of the $BaCO_3$ nanoparticles in LSCF electrode a) before long-term test, b) after long-term test

Single cell performance

A LSCF electrode with the optimized $BaCO_3$ loading (8.74 wt.%) was used as a cathode for the single cell testing. The tri-layer structured membrane of the single cell is displayed in Figure 5. The electrolyte is nearly 60 μm thick and densely structured which ensure the high open voltage of the single cell. It was noted that $BaCO_3$ nanoparticles distributed on the LSCF backbone with approximately the same size as

was observed in the symmetrical cell studies. Open pores were observed in the supporting substrate which should be beneficial to gas diffusion during the electrode reaction processes.

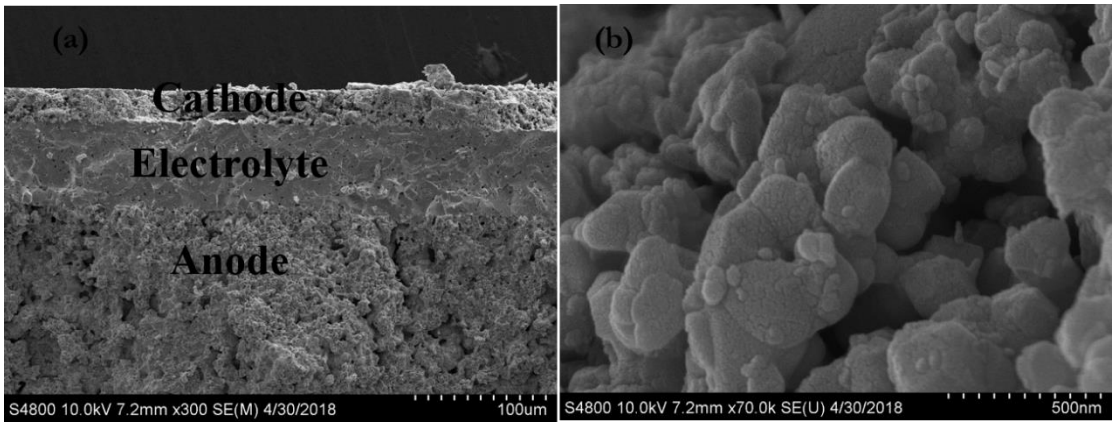

Figure 5. The microstructure of a) the single cell and LSCF electrode with $BaCO_3$ nanoparticles

Figure 6 shows the typical cell voltages (V) and powder density (P) as a function of current densities(J). The maximum power densities of the LSCF electrode with no $BaCO_3$ loadings was 268, 199, 118 and 58 mW•cm^{-2} at 700, 650, 600 and 550 ºC, respectively. The results are comparable to Amir R. Hanifi's [21] study, using 10 um BCZYYb as the electrolyte and LSCF as the cathode (166, 218 and mW•cm^2 at 600, 650 and 700 ºC, respectively). The maximum powder densities increased nearly 50% with the addition of the optimized $BaCO_3$ loadings (8.74 wt.%) (404, 312, 217 and 135 mW•cm^{-2} at 700, 650, 600 and 550 ºC, respectively). The increased maximum power density is due to the catalytic effect of the deposited $BaCO_3$ nanoscale particles on the LSCF backbone.

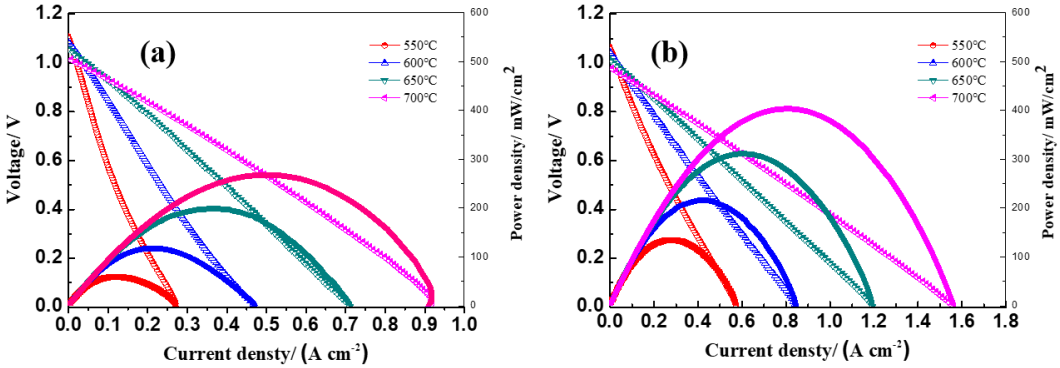

Figure 6. Voltage and power density versus current density for a) bare LSCF electrode, b) composite electrode with 8.7 wt.% $BaCO_3$ nanoparticles

Figure 7a and b shows the electrochemical impedance spectra for the single cells measured at between 550°C and 700°C. The equivalent circuit used for data fitting is shown in Fig. 7d. R0 is the serial resistance due to the electrolyte, electrodes, and connection wires; L1 is the inductance; R1-CPE1, R2-CPE2, and R3-CPE3 are the electrode resistive elements corresponding to the high-, mid-, and low-frequency arcs, respectively. It is evident that the polarization resistance was significantly reduced for the optimized LSCF cathode. According to high-resolution impedance study for anode-supported cells, the arc in the mid-frequency range (i.e., from 3 Hz to 300 Hz) is associated with cathode activation polarization.23 The equivalent circuit model analysis confirmed that the reduction in the total

polarization resistance for the single cell with the optimized cathode originated from cathode activation, as presented in Fig. 7c for the mid-frequency resistance (R2), suggesting that the BaCO3 nanoparticles effectively improved the ORR activity of the bare LSCF cathode.

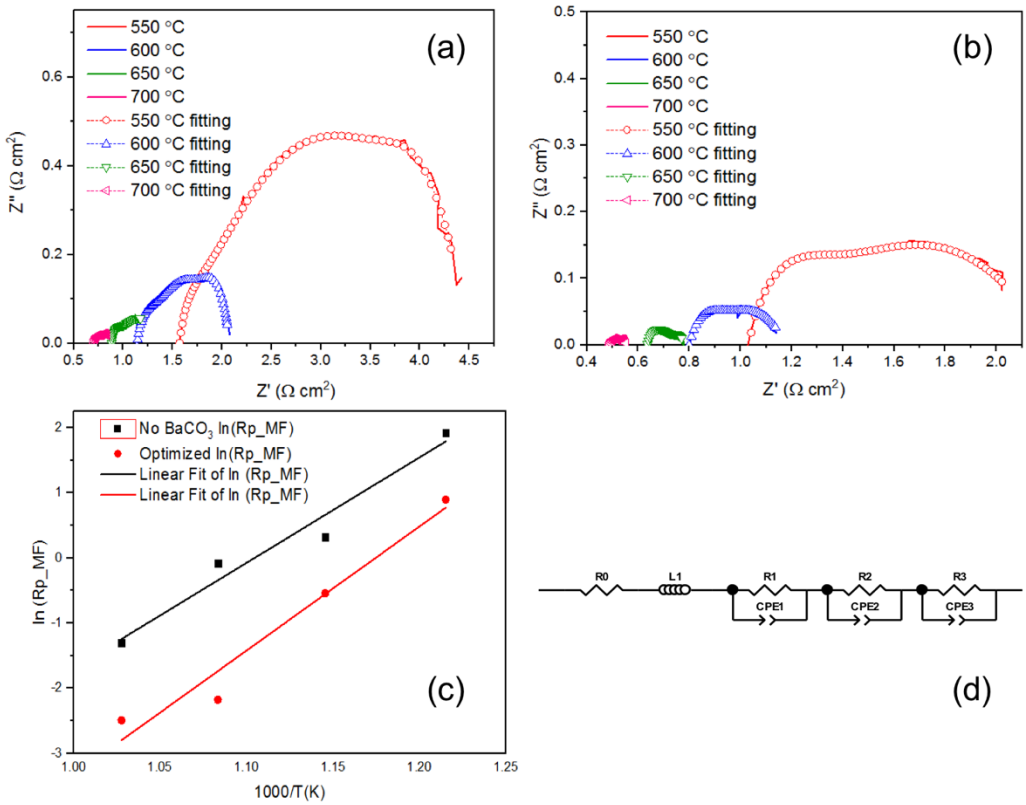

Figure 7. Electrochemical impedance spectra measure from 700 to 550° ºC for (a) single cell with bare LSCF electrode, (b) single cell with optimized LSCF electrode, (c) Arrhenius plot of polarization resistance from cathode for bare single cell and optimized single cell, (d) equivalent circuit for fitting the impedance spectra.

Conclusions

$BaCO_3$ nanoparticles were deposited on LSCF electrodes by a wet-chemistry infiltration method for enhanced performance of proton ceramic SOFCs. The catalytic effects were determined by using an LSCF electrode with varying amount of barium carbonate loading. The polarization resistance of the electrode decreased nearly 75% (from 1.123 to 0.293 Ω•cm^2 at 700 ºC) mainly due to the low-frequency polarization resistance which corresponding to the surface reaction process. The optimized symmetrical cell exhibited good chemical stability and physical stability with limited coarsening observed after extended tests for 300 h. The maximum power density increased 50% (from 268 to 404 mW•cm^{-2} at 700 ºC). $BaCO_3$ demonstrated promising performance enhancements of LSCF electrodes in H-SOFCs and warrants further testing on additional cathode systems.

Acknowledgement

KSB was supported in part by an appointment to the National Energy Technology Laboratory Research Participation Program, sponsored by the U.S. Department of Energy and administered by the Oak Ridge

Institute for Science and Education. We also gratefully acknowledge the financial support from the Department of Energy, Nuclear Energy Research Program (DOE-NEUP) Project: 17-12798: Nanostructured Ceramic Membranes for Enhanced Tritium Management**.**

Reference

1. N. Q. Minh, Journal of the American Ceramic Society **76**, 563 (1993).
2. Z. Zhan, Science **308**, 844 (2005).
3. S. Park, J. M. Vohs, and R. J. Gorte, **404**, 3 (2000).
4. S. M. Haile, Acta Materialia **51**, 5981 (2003).
5. E. Fabbri, L. Bi, D. Pergolesi, and E. Traversa, Advanced Materials **24**, 195 (2012).
6. Z. Shao and S. M. Haile, **431**, 4 (2004).
7. J. Gao, X. Meng, T. Luo, H. Wu, and Z. Zhan, International Journal of Hydrogen Energy **42**, 18499 (2017).
8. S. P. Jiang, International Journal of Hydrogen Energy **37**, 449 (2012).
9. X. Liu, H. Wu, Z. He, J. Gao, X. Meng, T. Luo, C. Chen, and Z. Zhan, International Journal of Hydrogen Energy **42**, 18410 (2017).
10. S. Jiang, Solid State Ionics **146**, 1 (2002).
11. E. Perry Murray, Solid State Ionics **148**, 27 (2002).
12. L. Lei, Z. Tao, T. Hong, X. Wang, and F. Chen, Journal of Power Sources **389**, 1 (2018).
13. G. Li, B. He, Y. Ling, J. Xu, and L. Zhao, International Journal of Hydrogen Energy **40**, 13576 (2015).
14. B. He, L. Zhang, Y. Zhang, D. Ding, J. Xu, Y. Ling, and L. Zhao, Journal of Power Sources **287**, 170 (2015).
15. T. Hong, K. S. Brinkman, and C. Xia, ChemElectroChem **3**, 805 (2016).
16. M. Li, Z. Sun, W. Yang, T. Hong, Z. Zhu, Y. Zhang, X. Wu, and C. Xia, Physical Chemistry Chemical Physics **19**, 503 (2017).
17. L. Zhang, T. Hong, Y. Li, and C. Xia, International Journal of Hydrogen Energy **42**, 17242 (2017).
18. Y. Yang, M. Li, Y. Ren, Y. Li, and C. Xia, International Journal of Hydrogen Energy **43**, 3797 (2018).
19. J. Martynczuk, M. Arnold, H. Wang, J. Caro, and A. Feldhoff, Advanced Materials **19**, 2134 (2007).
20. C. Duan, J. Tong, M. Shang, S. Nikodemski, M. Sanders, S. Ricote, A. Almansoori, and R. OHayre, Science **349**, 1321 (2015).
21. A. R. Hanifi, N. K. Sandhu, T. H. Etsell, and P. Sarkar, Journal of the American Ceramic Society **100**, 4983 (2017).